Inorganic Chemistry

pubs.acs.org/IC

Article

# Stable and Efficient Upconversion Single Red Emission from $CsPbI_3$ Perovskite Quantum Dots Triggered by Upconversion Nanoparticles

Yongsheng Zhu,[§] Jun Zhao,[§] Xueguo Li, Xiumei Xu, Jinshu Huang, Xiaoxu Ji, Gang Yang,* and Gencai Pan*

Cite This: *Inorg. Chem.* 2021, 60, 2649−2655

Read Online

ACCESS | Metrics & More | Article Recommendations | Supporting Information

**ABSTRACT:** Here, composites including highly efficient inert shell-modified $NaYF_4$:Yb/Tm@$NaYF_4$ upconversion nanoparticles (UCNPs) and $CsPbI_3$ perovskite quantum dots (PQDs) have been successfully synthesized by the assistance of (3-aminopropyl)-triethoxysilane (APTES) as a precursor for a $SiO_2$ matrix. UCNPs and $CsPbI_3$ PQDs in this composite structure show excellent stability in ambient conditions. Importantly, the efficient UC emission of $CsPbI_3$ PQDs was realized, which means that the single red emission of inert shell-modified UCNPs can be easily obtained by depending on these composite structures. Furthermore, the single red emission wavelength can be easily regulated from 705 to 625 nm by introducing appropriate proportion of $Br^-$ ions, which is very difficult to achieve for traditional UCNPs. Moreover, benefiting from the efficient downshifting (DS) red emission of $CsPbI_3$ PQDs, the composites possess the dual-wavelength excitation characteristics. So, the excellent dual-mode anticounterfeiting application has been demonstrated. This work will provide a new idea for the development of perovskite-based multifunctional materials.

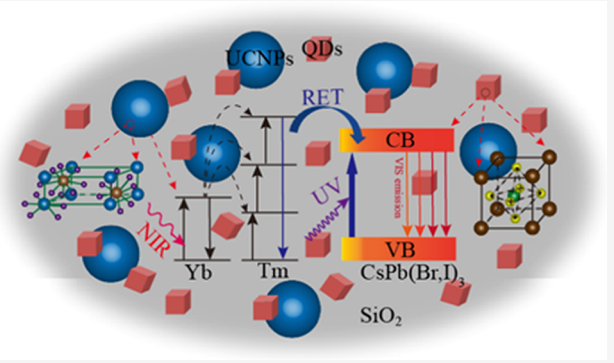




## INTRODUCTION

Controlling emission chromatography of trivalent rare-earth-doped upconversion nanocrystals (UCNPs) is crucial for their applications in the fields of sensing, biodetection, and anticounterfeiting.[1−8] Among others, Yb/Tm- and Yb/Er-codoped $NaYF_4$ exhibit a strong blue and green emission, respectively.[9−11] However, the inevitable overlap of the emission spectrum is the bottleneck of rare-earth-doped UCNPs, which greatly reduces the effect of the applications of photonic markers.[12] In contrast, all-inorganic lead halide perovskite quantum dots (PQDs) possess superior optical performance, such as large absorption cross section, high photoluminescence (PL) quantum yields (PLQYs), and high color purity.[13−20] These make them have great potential in promising applications including lighting, display, and anticounterfeiting.[14,21−23] However, the stability of PQDs is extremely poor when exposed to oxygen and water, especially $CsPbI_3$ PQDs with red emission.[19] Simultaneously, due to the absence of intermediate energy levels and low multiphoton absorption efficiency (<10 to 8), it is difficult to realize the nonlinear UC emission in $CsPbI_3$ PQDs.[23,24] Considering the advantages and disadvantages of these two materials, combining these two types of materials together may be able to solve their intrinsic drawbacks, and it is of significance to investigate the optical mechanism of the composites containing these two kinds of materials.

Recently, upconversion emission in PQDs has been realized by reabsorption from Yb/Tm:$LiYF_4$ nanoparticles (NPs) by physical mixing in a colloidal solution, which benefits from the superior optical properties of PQDs.[25] However, physical mixing in the colloidal state limits its practical applications. Furthermore, Tm:$NaYbF_4$ and $CsPbBr_3$ dual-phase NPs were embedded in glass, which realized the upconversion emission of $CsPbBr_3$ nanocrystals (NCs).[26] It is proved that the problem of poor long-term stability of NCs can be solved by embedding perovskite NCs into solid inorganic oxide glass. At the same time, the photon UC of $CsPbX_3$ PQDs was realized by mixing $CsPbX_3$ PQDs and Tm:$KYb_2F_7$ UCNPs in glass, which endows PQDs with long-term stability against decomposition.[27] However, the research on the composite of PQDs and UCNPs is still in its infancy. To our knowledge, the composite of UCNPs and $CsPbI_3$ PQDs embedded in the $SiO_2$ matrix has not been reported.

In this work, (3-aminopropyl)triethoxysilane (APTES) has been slowly hydrolyzed to form the silica protection matrix for

**Received:** December 1, 2020
**Published:** January 31, 2021

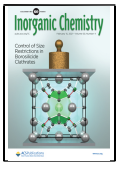







https://dx.doi.org/10.1021/acs.inorgchem.0c03516
*Inorg. Chem.* 2021, 60, 2649−2655

PQDs and UCNPs. In this way, the composites including highly efficient $NaYF_4$:Yb/Tm@$NaYF_4$ UCNPs and $CsPbI_3$ PQDs have been formed. Also, the silica matrix can greatly improve the stability of $CsPbI_3$ PQDs in ambient conditions. More importantly, the UC single red emission of $CsPbI_3$ PQDs was realized. Moreover, the single red emission wavelength can be easily regulated from 705 to 625 nm by anion exchange, which is very difficult to achieve in UCNPs. Moreover, benefiting from the dual-wavelength excitation characteristics, the composite has been successfully applied to dual-mode anticounterfeiting.

## EXPERIMENTS

**Chemicals.** NaOH (AR), $NH_4F$ (AR), methanol (AR), ethanol (AR), hydrochloric acid (AR), and 1-octadecene (ODE, AR) were purchased from Sinopharm Chemical Reagent Co., Ltd., China. $PbI_2$, $PbBr_2$, $Y_2O_3$, $Yb_2O_3$, and $Tm_2O_3$ with the same purity of 99.99% and $Cs_2CO_3$ (99.9%), oleic acid (OA, 90%), oleylamine (OLA, 90%), cyclohexane, and (3-aminopropyl)triethoxysilane (98%, APTES) were provided by Aladdin, China.

**Synthesis of $CsPbI_3$ and $CsPb(Br,I)_3$ PQDs.** First, a cesium oleate precursor solution was prepared. $Cs_2CO_3$ (0.8 g), 2 mL of OA, and 20 mL of ODE were placed in a three-necked flask and degassed for 10 min. The solution was then heated to 120 °C under a $N_2$ flow atmosphere with constant stirring for 40 min until a clear solution was obtained. Next, $PbI_2$ (0.376 mmol), OLA (1 mL), OA (1 mL), and ODE (15 mL) were added to another flask and stirred under purging $N_2$ flow. The temperature was kept at 120 °C for 1 h until the adequate dissolution of $PbI_2$. Then, the temperature was increased to a required value of 160 °C, the as-prepared Cs-oleate (1 mL) was swiftly injected, and just after 30 s, the solution was cooled down to room temperature by an ice bath. The PQDs were purified by centrifugation and then dissolved in 4 mL of cyclohexane. Different amounts of $PbBr_2$ were added to synthesize $CsPb(Br,I)_3$ PQDs using the same method.

**Synthesis of Core/Shell $NaYF_4$:Yb/Tm@$NaYF_4$ UCNPs.** The NaYF4:Yb/Tm cores were prepared via a typical solvothermal method as described in our previous work.[28] The doped concentrations of $Tm^{3+}$ and $Yb^{3+}$ ions were kept as 0.5 and 20 mol %, respectively. The same method was used to fabricate core/shell $NaYF_4$:Yb/Tm@$NaYF_4$ UCNPs, in which the preprepared $NaYF_4$:Yb/Tm cores dispersed in 4 mL of cyclohexane were added to the solution before the addition of 10 mL of methanol solution and kept at room temperature for 10 min. The samples were purified and dispersed in 4 mL of cyclohexane.

**Synthesis of PQD/UCNP Composites.** The procedure of the synthesis of PQD/UCNP composites was similar to the synthesis of PQDs, and the experimental details can be found in Supporting Information. After the adequate dissolution of $PbI_2$ and $PbBr_2$, the appropriate amounts of NaYF4:Yb/Tm@$NaYF_4$ UCNPs were added to the solution. In addition, 50 uL of OA and 1 mL of APTES were slowly added to the flask before the temperature was increased to 160 °C. When the resulting solution was cooled down to room temperature by an ice bath, the flask was exposed to air and stirred for 1 h in a water bath (60 °C and 50% humidity) for hydrolysis; the PQDs and UCNPs were well encapsulated in an organic silica matrix formed by silanization.

**Characterization.** The morphologies of the samples were characterized by transmission electron microscopy (TEM) (JEOL-JEM-2100, JP). High-resolution TEM (HRTEM) imaging, energy-dispersive X-ray (EDX) analysis, and elemental mapping were performed by an energy dispersion detector operating at 200 kV. Crystalline characteristics of the samples were also analyzed by X-ray diffraction (XRD) with Cu K$\alpha$ radiation ($\lambda$ = 1.5406 Å). The absorption spectra were measured using a Shimadzu UV-3101PC scanning spectrophotometer. The PL/upconversion luminescence (UCL) spectra and decay lifetimes were measured using an Edinburgh fluorescence spectrometer (FLS1000). PLQYs and upconversion quantum yields (UCQYs) were measured by integrating an integrating sphere in the fluorescence spectrometer. All of the measurements were carried out at room temperature. The photographs were taken with a digital camera without any ornament.

## RESULTS AND DISCUSSION

The morphologies of all as-synthesized samples were first characterized by transmission electron microscopy (TEM). As shown in Figure 1a and the inset, $CsPbI_3$ PQDs show a typical

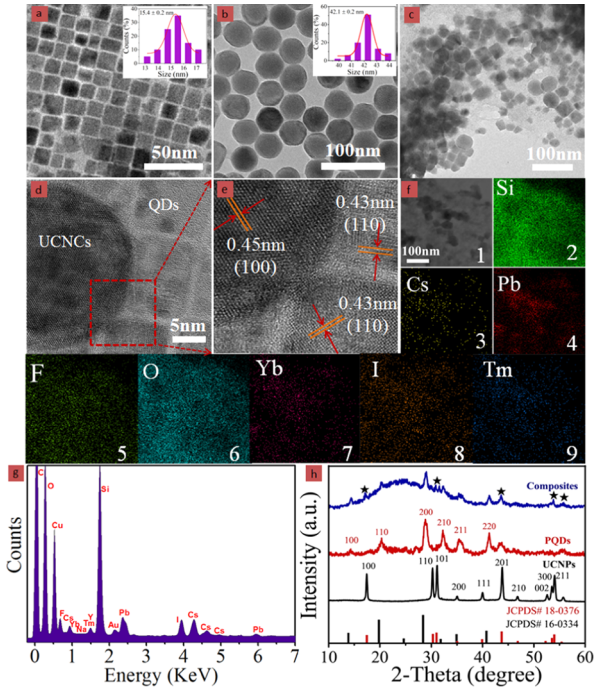


**Figure 1.** (a, b) Typical transmission electron microscopy (TEM) images of the as-synthesized $CsPbI_3$ PQDs and $NaYF_4$:Yb/Tm@$NaYF_4$ UCNPs, respectively; the insets show the size distribution of the PQDs and UCNPs; (c–e) TEM and high-resolution TEM (HRTEM) images of the PQD/UCNP composites encapsulated by $SiO_2$; (f) energy-dispersive X-ray (EDX) spectroscopy and (g) corresponding EDX elemental mapping of the composites; (h) XRD patterns of the pure $CsPbI_3$ PQDs, $NaYF_4$:Yb/Tm@$NaYF_4$ UCNPs, and PQD/UCNP composites with a molar ratio of 1:0.25. The standard data of $NaYF_5$ (JCPDS No. 16-0334) and $CsPbI_3$ (JCPDS No. 18-0376) are also given for reference.

cubic shape, and the average size is about 15.4 nm. Uniformly distributed hexagonal particles were observed for $NaYF_4$:Yb/Tm cores and core/shell $NaYF_4$:Yb/Tm@$NaYF_4$ UCNPs, as shown in Figures 1b andS1. The sizes of core/shell structured UCNPs (42.1 nm) were obviously larger than that of $NaYF_4$:Yb/Tm cores (36.3 nm). As for the composites, $CsPbI_3$ PQDs were successfully encapsulated in $SiO_2$ together with the core/shell structured UCNPs (Figures 1c andS2), and the PQDs were mainly gathered around the surface of UCNPs, as shown in Figure 1d. In addition, these two kinds of nanoparticles both good crystallinity, as evidenced by two clear different lattice fringes observed in the high-resolution transmission electron microscopy (HRTEM) image (Figure 1e); the lattice fringes with an interplanar distance of 0.45 nm were assigned to the (100) crystal planes of the UCNPs, and another interplanar distance of 0.43 nm belonged to the (110) planes of $CsPbI_3$ PQDs. The chemical compositions of the composites sample were analyzed by energy-dispersive X-ray


https://dx.doi.org/10.1021/acs.inorgchem.0c03516
Inorg. Chem. 2021, 60, 2649–2655

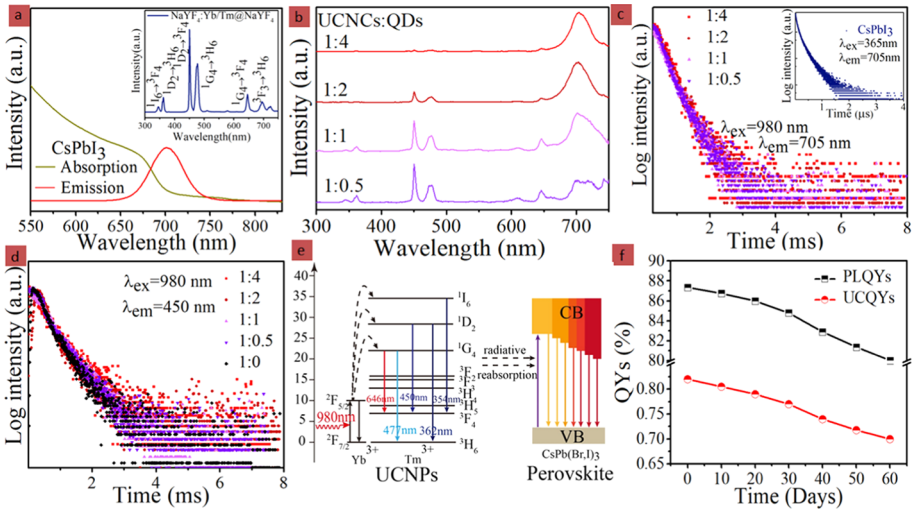


**Figure 2.** (a) Absorption (black) and photoluminescence (PL) spectra (red) of $CsPbI_3$ PQDs; the insets show the upconversion luminescence (UCL) spectrum for the core/shell $NaYF_4$:Yb/Tm@$NaYF_4$ UCNPs; (b) UCL spectrum of the PQD/UCNP composites with varying PQD concentrations under 980 nm laser excitation; (c) fluorescence decay dynamics of PQD/UCNP composites with varying $CsPbI_3$ PQD concentrations by monitoring the emissions at 705 nm under 980 nm excitation; the inset shows PL decays of the as-synthesized $CsPbI_3$ PQDs; (d) UCL decays from $^1D_2$ of $Tm^{3+}$ by monitoring the emissions at 450 nm in PQD/UCNP composites with different PQD concentrations under 980 nm excitation; (e) schematic representation of the radiative energy transfer upconversion (RETU) processes in the PQD/UCNP composites; and (f) PLQYs/UCQYs of the composite samples under UV−near-infrared (NIR) excitation as a function of the storage time.

(EDX) elemental mapping (Figure 1f) and EDX spectroscopy (Figure 1g); all of the expected signals of Cs, Pb, I, Na, Y, F, Yb, Tm, Si, and O elements were identified. The raw atomic ratio data obtained by EDX analysis is shown in Table S1. The results confirmed the uniform distribution of Si and O in the samples, and the PQDs and UCNPs were successfully encapsulated in the silica matrix.

The results of the X-ray diffraction (XRD) measurements are depicted in Figure 1h. All of the diffraction peaks of the core/shell UCNPs matched well with the standard pattern of hexagonal $NaYF_4$ (JCPDS No.16-0334), indicating pure phase and high crystallinity of the resulting UCNPs. In addition, the cubic structure of the PQDs can be further confirmed compared with the standard pattern of cubic $CsPbI_3$ (JCPDS No. 18-0376). For the composite sample, diffraction peaks for both PQDs and UCNPs can be observed and the signals for PQDs dominate, which is because the XRD pattern of the composites was tested at 1:4 of UCNPs and $CsPbI_3$ QDs, namely, the number of UCNPs was relatively few in the composites. Moreover, the appearance of a broad wave at 20−30° illustrates the formation of amorphous $SiO_2$, corresponding to the EDX and TEM images. All of the above results confirm the successful synthesis of the $SiO_2$-coated PQD/UCNP composites in our experiment.

Figure 2a depicts the optical absorption and PL spectra ($\lambda_{ex}$ = 365 nm) of pure $CsPbI_3$ PQDs. Large absorption cross sections in the ultraviolet (UV) and visible spectral regions were confirmed, and therefore, the intense emission peak at about 705 nm with a bandwidth of 43 nm could be attributed to the exciton recombination of $CsPbI_3$ PQDs. A stokes shift of 20 nm was observed between the emission peak and the absorption peak. In addition, the inset of Figure 2a shows that the prepared core/shell UCNPs exhibited bright blue luminescence emission under the excitation of a 980 nm CW diode laser, which included a set of intense sharp and typical upconversion luminescence (UCL) emission peaks from $Tm^{3+}$. However, the UCL intensity was much lower for $NaYF_4$:Yb/Tm cores due to the surface quenching effect, as presented in Figure S3. Therefore, the core/shell structured UCNPs were selected as the excitation light source to excite the luminescence emission of the PQDs in this work. The UC QY of $NaYF_4$:Yb/Tm@$NaYF_4$ UCNPs was measured, and the value was 1.2%. To investigate the optimal utilization of emission from UCNPs, the PQD/UCNP composites with varying PQD concentrations (the molar ratio of UCNPs and PQDs varies from 1:0.5 to 1:4) were successfully synthesized, and the UCL spectra under 980 nm laser excitation are given in Figure 2b. With increasing concentration of PQDs, the emission at 705 nm for $CsPbI_3$ QDs enhanced gradually, while the emission peak of $Tm^{3+}$ vanished gradually, implying an efficient energy transfer from the UCNPs to PQDs. The much larger absorbance across $CsPbI_3$ QDs in the UV region leads to a much faster decrease of the emission intensities at 347 and 362 nm than that of the blue emissions at 450 and 477 nm. It should be noted that the UV and blue emissions almost queued absolutely when the molar ratio of UCNPs and PQDs reached 1:4, which means that the good upconversion of single red emission for the PQD/UCNP composites has been realized.

The fluorescence decay dynamics were investigated to gain more insights into the energy-transfer process. As shown in Figure 2c, the UCL decays from $CsPbI_3$ PQD/UCNP composites' emissions under 980 nm excitation present a single exponential behavior. All of the UCL lifetimes of $CsPbI_3$ PQDs were determined to be about hundreds of microseconds and were independent of the concentration of $CsPbI_3$ PQDs (Table S2). However, the PL decay curves of pure $CsPbI_3$ PQDs (inset of Figure 2c) can be well fitted with biexponential functions by the formula[19]

$$I(t) = I_1 \exp(-t/\tau_1) + I_2 \exp(-t/\tau_2) \quad (1)$$

The average PL lifetime of CsPbI3 PQDs was calculated to be 222.26 ns (Table S3), which is much shorter than their UCL lifetimes of exciton emissions in PQD/UCNP


https://dx.doi.org/10.1021/acs.inorgchem.0c03516
Inorg. Chem. 2021, 60, 2649−2655

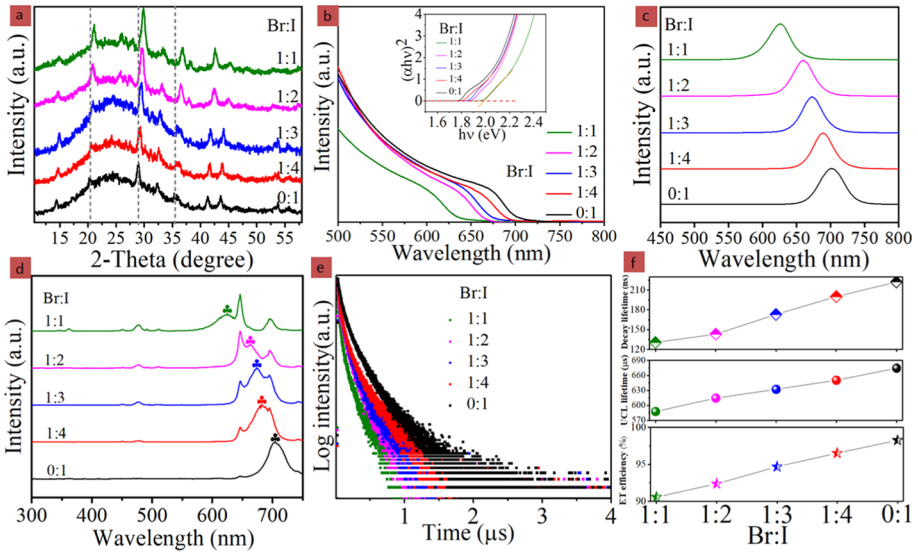


**Figure 3.** (a) XRD patterns of the composites using $CsPb(Br,I)_3$ PQDs with varying halide compositions; (b) optical absorption spectra of $CsPb(Br,I)_3$ PQDs with varying halide compositions; the inset shows the corresponding Tauc plots of $(\alpha h\nu)^2$ versus $h\nu$; (c) PL spectra of the $CsPb(Br,I)_3$ PQDs with varying halide compositions upon excitation by 365 nm UV light; (d) UCL emission spectra of the $CsPb(Br,I)_3$ PQD/UCNP composites under 980 nm laser excitation; (e) PL decay curves of the $CsPb(Br,I)_3$ PQDs upon excitation by a 365 nm picosecond laser; (f) evolution of the PL decay lifetimes, UCL lifetimes of the exciton recombination, and the calculated energy transfer efficiency versus halogen component in $CsPb(Br,I)_3$ PQD/UCNP composites.

composites. In addition, the UCL lifetimes of $Tm^{3+}$ emission at 450 nm also keep almost unchanged (about 600 $\mu$s) with varying PQD concentrations under 980 nm excitation (Figure 2d and Table S2). The above results indicate that the upconverted exciton emission from the PQD/UCNP composites is governed by a radiative photon reabsorption process rather than a nonradiative Förster resonance energy transfer (FRET) because FRET always results in a decrease in the lifetime of the energy donor by imposing an additional relaxation channel on the donor.[25] As schematically illustrated in Figure 2e, the $Yb^{3+}$ ions were first excited by NIR (980 nm) excitation and then the energy was transferred to $Tm^{3+}$ ions to obtain UC emission. These emission lights can be reabsorbed by red PQDs due to the large absorption cross section.[29] Therefore, the upconversion emission can be realized by photon emission through exciton recombination. Furthermore, the stability of the composites was largely improved due to the excellent protective effect of $SiO_2$, as depicted in Figure 2f; the PLQYs of the pure PQDs can maintain more than 80% after 60 days with an initial value of 87% during atmospheric environment monitoring. Likewise, the absolute upconversion quantum yields (UCQYs) for the composite sample only decrease by about 10% in ambient conditions. Furthermore, the pure $CsPbI_3$ QDs and the composites were put into two glass vials containing the same amount of ultrapure water, and the antiwater stability was monitored. The results showed that the antiwater stability of the composite structure is greatly improved compared with that of the bare $CsPbI_3$ QDs (Figure S4).

To realize upconversion single red emission with a tunable wavelength, $CsPb(Br,I)_3$ PQD/UCNP composites with varying halide compositions were further prepared (the molar ratios of UCNPs and PQDs were fixed as 1:4). XRD patterns shown in Figure 3a confirmed the continuous increase of $Br^-$ anions without destroying the crystal structures. The diffraction peaks for PQDs gradually shift toward larger angles, implying the fact that the larger $I^-$ ions in PQDs are gradually substituted by the smaller $Br^-$. Optical absorption spectra (Figure 3b) of the PQDs and the related Tauc plots (inset of Figure 3b) showed that the band edges shift to the higher energy side with increasing $Br^-$ concentration. The absorbance in the UV and visible spectral regions reduced somewhat, especially when the ratio of Br/I reached 1:1. The PL spectra recorded in Figure 3c indicate that the as-prepared $CsPb(Br,I)_3$ PQDs can yield single red emissions with a tunable wavelength from 625 to 705 nm under UV (365 nm) light excitation, which is consistent with the results of PQDs reported previously.[30] Also, the PLQYs of PQDs with different atomic ratios of Br to I are shown in Figure S5.

Furthermore, the UCL emission spectra of the $CsPb(Br,I)_3$ PQD/UCNP composites are shown in Figure 3d. As expected, the characteristic emissions assigned to exciton recombination of the $CsPb(Br,I)_3$ PQDs were dominant in the UCL spectra. However, the emissions of $Tm^{3+}$ were selectively quenched. In other words, the UV and blue emissions vanished gradually with increasing $I^-$ ions due to the intensifying absorbance of the PQDs in this region, but the red emissions at 648 and 700 nm cannot be absolutely absorbed or even cannot be absorbed in accordance with their absorption spectra. Whatever, the upconversion red emission from $CsPb(Br,I)_3$ PQDs was obtained and the wavelength can be tuned by adjusting the ratio of halogen elements. The PL decay curves of the $CsPb(Br,I)_3$ PQDs were fitted by a biexponential function (Figure 3e). The obvious decrease of the effective lifetimes from 222.26 to 130.27 ns with increasing $Br^-$ concentration was observed (Table S3). Although the UCL lifetimes of the $CsPb(Br,I)_3$ PQD/UCNP composites have the same varying tendency with different halogen element ratios (Figure 3f and Table S4), the apparently lengthened UCL lifetimes in contrast to the original PL lifetimes further confirm the radiative photon reabsorption process in the PQD/UCNP composites. In addition, the energy transfer efficiency ($\eta^{ET}$) defined as the ratio of photon numbers absorbed by PQDs ($n_{abs}$) to the total photon numbers with energies larger than the band edge of


https://dx.doi.org/10.1021/acs.inorgchem.0c03516
Inorg. Chem. 2021, 60, 2649−2655

PQDs ($n_{em}$) in pure UCNPs can be calculated from the UCL emission spectra using the following formula[25]

$$\eta^{ET} = \frac{I_0^{Tm} - I_x^{Tm}}{I_0^{Tm}} \quad (2)$$

where $I_0^{Tm}$ and $I_x^{Tm}$ represent the integrated intensities of the UCL of $Tm^{3+}$ with frequencies above the band edges of $CsPb(Br,I)_3$ PQDs in the pure UCNPs and PQD/UCNP composites, respectively. The variation trends of calculated $\eta^{ET}$ are also depicted in Figure 3f. The highest $\eta^{ET}$ from the UCNPs to pure $CsPbI_3$ can be ascribed to their relatively higher absorbance compared to $CsPb(Br,I)_3$ PQDs.

Through the above analysis of the PL and UCL spectra, it can be concluded that the PQD/UCNP composites encapsulated in $SiO_2$ can be simultaneously excited by routine UV light and near-infrared (NIR) light. Moreover, the stability was dramatically improved due to the protective effect of $SiO_2$, even though the composites were dried to a solid state. Figure 4a shows the luminescent photographs of the powders and solutions upon UV and NIR light irradiation. Benefiting from the dual-wavelength excitation characteristics of the composites, the promising application of anticounterfeiting was proposed.

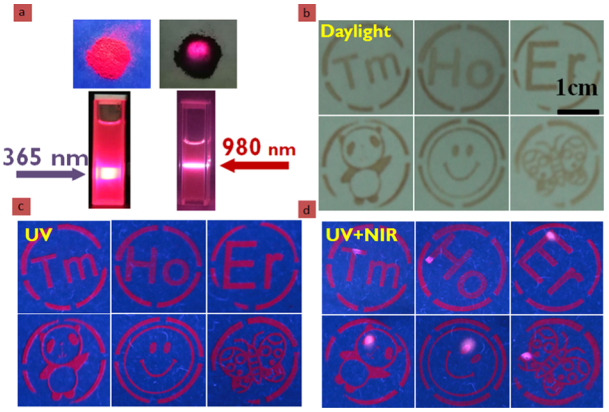


**Figure 4.** (a) Luminescent photographs of the $CsPbI_3$ PQD/UCNP composite powders and solutions upon UV and NIR light irradiation. (b–d) Photographs of anticounterfeiting patterns printed on paper irradiated by daylight, 365 nm UV light, and concurrent UV light and NIR laser (980 nm), respectively.

To realize the display of dual anticounterfeiting application, uniform mixtures of ink were prepared by mixing the as-prepared $CsPbI_3$ PQD/UCNP composites with blank screen-printing ink, and a series of luminescent patterns were designed and printed on a paper via the screen printing technique as reported.[31−33] Then, these patterns were irradiated by different diverse excitation modes, such as daylight (Figure 4b), 365 nm UV light (Figure 4c), and concurrent UV light and 980 nm NIR laser (Figure 4d). Compared to the case under daylight conditions, bright red emissions were distinctly observed when exposed to 365 nm UV light. More importantly, in the regions that were simultaneously irradiated by the 980 NIR laser, the UC emission colors superpose the corresponding PL patterns, and the pink patterns were identified. The stability of the anticounterfeiting pattern has been monitored (Figure S6), and the result indicates that the security pattern did not change much after 15 days. These results confirm that stable PQD/UCNP composites have great potential in dual-model anticounterfeiting and other related applications.

## CONCLUSIONS

In summary, the composites of PQDs/UCNPs coated by $SiO_2$ were synthesized by slowly hydrolyzing the APTES capping agent in situ. The composites possessed good stability in air. More importantly, benefiting from the dual-wavelength excitation characteristics, the composites were successfully applied to dual-mode anticounterfeiting. This work indicates that the development of perovskite-based composite materials can provide more application space for perovskite materials.

## ASSOCIATED CONTENT

### Supporting Information

The Supporting Information is available free of charge at https://pubs.acs.org/doi/10.1021/acs.inorgchem.0c03516.

Experimental details; TEM images of UCNPs and composites; spectra of UCNPs; stability of composites; PLQYs; stability of anticounterfeiting patterns; atomic ratio data by EDX analysis; comparison of UC decay lifetimes from exciton recombination and $^1D_2$ of $Tm^{3+}$ by monitoring the emissions at 450 nm in $CsPbI_3$ PQD/UCNP composites with varying PQD concentrations; time-resolved PL decay profiles for $CsPb(Br,I)_3$ PQDs with varying halide compositions; and comparison of DS (PL) and UC decay lifetimes of exciton recombination from $CsPb(Br,I)_3$ PQD/UCNP composites with varying halogen compositions (PDF)

## AUTHOR INFORMATION

### Corresponding Authors

**Gang Yang** − *Henan International Joint Laboratory of MXene Materials Microstructure, College of Physics and Electronic Engineering, Nanyang Normal University, Nanyang 473061, P. R. China*; Email: nynuyanggang@163.com

**Gencai Pan** − *School of Physics and Electronics, Henan University, Kaifeng 475004, P. R. China*; orcid.org/0000-0001-5969-2679; Email: pangencai@126.com

### Authors

**Yongsheng Zhu** − *Henan International Joint Laboratory of MXene Materials Microstructure, College of Physics and Electronic Engineering, Nanyang Normal University, Nanyang 473061, P. R. China*

**Jun Zhao** − *School of Physics and Electronics, Henan University, Kaifeng 475004, P. R. China*

**Xueguo Li** − *Henan International Joint Laboratory of MXene Materials Microstructure, College of Physics and Electronic Engineering, Nanyang Normal University, Nanyang 473061, P. R. China*

**Xiumei Xu** − *Henan International Joint Laboratory of MXene Materials Microstructure, College of Physics and Electronic Engineering, Nanyang Normal University, Nanyang 473061, P. R. China*; orcid.org/0000-0001-6432-8732

**Jinshu Huang** − *Henan International Joint Laboratory of MXene Materials Microstructure, College of Physics and Electronic Engineering, Nanyang Normal University, Nanyang 473061, P. R. China*

**Xiaoxu Ji** − *Henan International Joint Laboratory of MXene Materials Microstructure, College of Physics and Electronic*



https://dx.doi.org/10.1021/acs.inorgchem.0c03516
Inorg. Chem. 2021, 60, 2649−2655

*Engineering, Nanyang Normal University, Nanyang 473061, P. R. China*

Complete contact information is available at: https://pubs.acs.org/10.1021/acs.inorgchem.0c03516

### Author Contributions

[§]Y.Z. and J.Z. contributed equally to this work.

### Notes

The authors declare no competing financial interest.

## ■ ACKNOWLEDGMENTS

This work was sponsored by the National Natural Science Foundation of China (Grant Nos. U1904178, 51802163, and 61703216), the Natural Science Foundation of Henan Province (No. 202300410297, 202300410295), the Program for Science & Technology Innovation Talents in Universities of Henan Province (No. 19HASTIT019), the Science and Technology Project of Henan Province (No. 182102210466), and the Youth Project of Nanyang Normal University (No. 2020QN016). This work was also supported by the Open Fund of the State Key Laboratory on Integrated Optoelectronics (Grant No. IOSKL2017KF10).

## ■ REFERENCES

(1) Chen, X.; Xu, W.; Zhang, L.; Bai, X.; Cui, S.; Zhou, D.; Yin, Z.; Song, H.; Kim, D.-H. Large Upconversion Enhancement in the "Islands" Au−Ag Alloy/$NaYF_4$: $Yb^{3+}$, $Tm^{3+}$/$Er^{3+}$ Composite Films, and Fingerprint Identification. *Adv. Funct. Mater.* **2015**, *25*, 5462−5471.

(2) Ding, M.; Dong, B.; Lu, Y.; Yang, X.; Yuan, Y.; Bai, W.; Wu, S.; Ji, Z.; Lu, C.; Zhang, K.; Zeng, H. Energy Manipulation in Lanthanide-Doped Core−Shell Nanoparticles for Tunable Dual-Mode Luminescence toward Advanced Anti-Counterfeiting. *Adv. Mater.* **2020**, No. 2002121.

(3) Dong, B.; Cao, B. S.; He, Y. Y.; Liu, Z.; Li, Z. P.; Feng, Z. Q. Temperature sensing and in vivo imaging by molybdenum sensitized visible upconversion luminescence of rare-earth oxides. *Adv. Mater.* **2012**, *24*, 1987−1993.

(4) Wang, L.; Yan, R.; Huo, Z.; Wang, L.; Zeng, J.; Bao, J.; Wang, X.; Peng, Q.; Li, Y. Fluorescence resonant energy transfer biosensor based on upconversion-luminescent nanoparticles. *Angew. Chem., Int. Ed.* **2005**, *44*, 6054−6057.

(5) Zhou, L.; Wang, R.; Yao, C.; Li, X. M.; Wang, C. L.; Zhang, X. Y.; Xu, C. J.; Zeng, A. J.; Zhao, D. Y.; Zhang, F. Single-band upconversion nanoprobes for multiplexed simultaneous in situ molecular mapping of cancer biomarkers. *Nat. Commun.* **2015**, *6*, No. 6938.

(6) Chen, J.; Wang, S.; Lin, J.; Chen, D. CsRe2F7@glass nanocomposites with efficient up-/down-conversion luminescence: from in situ nanocrystallization synthesis to multi-functional applications. *Nanoscale* **2019**, *11*, 22359−22368.

(7) Huang, H.; Chen, J. K.; Liu, Y. T.; Lin, J. D.; Wang, S. X.; Huang, F.; Chen, D. Q. Lanthanide-Doped Core@Multishell Nanoarchitectures: Multimodal Excitable Upconverting/Downshifting Luminescence and High-Level Anti-Counterfeiting. *Small* **2020**, *16*, No. 2000708.

(8) Wang, S.; Lin, J.; He, Y.; Chen, J.; Yang, C.; Huang, F.; Chen, D. Remarkable laser-driven upconverting photothermal effect of Cs3LnF6@glass nanocomposites for anti-counterfeiting. *Chem. Eng. J.* **2020**, *394*, No. 124889.

(9) Wang, F.; Han, Y.; Lim, C. S.; Lu, Y.; Wang, J.; Xu, J.; Chen, H.; Zhang, C.; Hong, M.; Liu, X. Simultaneous phase and size control of upconversion nanocrystals through lanthanide doping. *Nature* **2010**, *463*, 1061−1065.

(10) Yi, G. S.; Chow, G. M. Synthesis of Hexagonal-Phase $NaYF_4$:Yb,Er and NaYF4:Yb,Tm Nanocrystals with Efficient Up-Conversion Fluorescence. *Adv. Funct. Mater.* **2006**, *16*, 2324−2329.

(11) Yin, Z.; Li, H.; Xu, W.; Cui, S.; Zhou, D.; Chen, X.; Zhu, Y.; Qin, G.; Song, H. Local Field Modulation Induced Three-Order Upconversion Enhancement: Combining Surface Plasmon Effect and Photonic Crystal Effect. *Adv. Mater.* **2016**, *28*, 2518−2525.

(12) Tian, G.; Gu, Z.; Zhou, L.; Yin, W.; Liu, X.; Yan, L.; Jin, S.; Ren, W.; Xing, G.; Li, S.; Zhao, Y. $Mn^{2+}$ Dopant-Controlled Synthesis of $NaYF_4$:Yb/Er Upconversion Nanoparticles for in vivo Imaging and Drug Delivery. *Adv. Mater.* **2012**, *24*, 1226−1231.

(13) Liu, Y.; Li, F.; Liu, Q. L.; Xia, Z. G. Synergetic Effect of Postsynthetic Water Treatment on the Enhanced Photoluminescence and Stability of $CsPbX_3$ (X = Cl, Br, I) Perovskite Nanocrystals. *Chem. Mater.* **2018**, *30*, 6922−6929.

(14) Pan, G.; Bai, X.; Xu, W.; Chen, X.; Zhai, Y.; Zhu, J.; Shao, H.; Ding, N.; Xu, L.; Dong, B.; Mao, Y.; Song, H. Bright Blue Light Emission of $Ni^{2+}$ Ion-Doped $CsPbClxBr_3$−x Perovskite Quantum Dots Enabling Efficient Light-Emitting Devices. *ACS Appl. Mater. Interfaces* **2020**, *12*, 14195−14202.

(15) Pan, G.; Bai, X.; Yang, D.; Chen, X.; Jing, P.; Qu, S.; Zhang, L.; Zhou, D.; Zhu, J.; Xu, W.; Dong, B.; Song, H. Doping lanthanide into perovskite nanocrystals: highly improved and expanded optical properties. *Nano lett.* **2017**, *17*, 8005−8011.

(16) Protesescu, L.; Yakunin, S.; Bodnarchuk, M. I.; Krieg, F.; Caputo, R.; Hendon, C. H.; Yang, R. X.; Walsh, A.; Kovalenko, M. V. Nanocrystals of Cesium Lead Halide Perovskites ($CsPbX_3$, X = Cl, Br, and I): Novel Optoelectronic Materials Showing Bright Emission with Wide Color Gamut. *Nano lett.* **2015**, *15*, 3692−3696.

(17) Shi, Z. F.; Li, Y.; Zhang, Y. T.; Chen, Y. S.; Li, X. J.; Wu, D.; Xu, T. T.; Shan, C. X.; Du, G. T. High-efficiency and air-stable perovskite quantum dots light-emitting diodes with an all-inorganic heterostructure. *Nano lett.* **2017**, *17*, 313−321.

(18) Sun, C.; Zhang, Y.; Ruan, C.; Yin, C.; Wang, X.; Wang, Y.; Yu, W. W. High-efficiency and air-stable perovskite quantum dots light-emitting diodes with an all-inorganic heterostructure. *Adv. Mater.* **2016**, *28*, 10088−10094.

(19) Zhu, Y.; Zhao, J.; Yang, G.; Xu, X.; Pan, G. Ammonium acetate passivated $CsPbI_3$ perovskite nanocrystals for efficient red light-emitting diodes. *Nanoscale* **2020**, *12*, 7712−7719.

(20) Pan, G.; Bai, X.; Xu, W.; Chen, X.; Zhou, D.; Zhu, J.; Shao, H.; Zhai, Y.; Dong, B.; Xu, L.; Song, H. Impurity ions codoped cesium lead halide perovskite nanocrystals with bright white light emission toward ultraviolet−white light-emitting diode. *ACS Appl. Mater. Interfaces* **2018**, *10*, 39040−39048.

(21) Xu, L.; Chen, J.; Song, J.; Li, J.; Xue, J.; Dong, Y.; Cai, B.; Shan, Q.; Han, B.; Zeng, H. Double-protected all-inorganic perovskite nanocrystals by crystalline matrix and silica for triple-modal anti-counterfeiting codes. *ACS Appl. Mater. Interfaces* **2017**, *9*, 26556−26564.

(22) Chen, D.; Chen, X. Luminescent perovskite quantum dots: synthesis, microstructures, optical properties and applications. *J. Mater. Chem. C* **2019**, *7*, 1413−1446.

(23) Deutsch, Z.; Neeman, L.; Oron, D. Luminescence upconversion in colloidal double quantum dots. *Nat. Nanotechnol.* **2013**, *8*, 649−653.

(24) Wang, Y.; Li, X.; Zhao, X.; Xiao, L.; Zeng, H.; Sun, H. Nonlinear absorption and low-threshold multiphoton pumped stimulated emission from all-inorganic perovskite nanocrystals. *Nano lett.* **2016**, *16*, 448−453.

(25) Zheng, W.; Huang, P.; Gong, Z.; Tu, D.; Xu, J.; Zou, Q.; Li, R.; You, W.; Bunzli, J. G.; Chen, X. Near-infrared-triggered photon upconversion tuning in all-inorganic cesium lead halide perovskite quantum dots. *Nat. Commun.* **2018**, *9*, No. 3462.

(26) Li, X.; Yang, C.; Yu, Y.; Li, Z.; Lin, J.; Guan, X.; Zheng, Z.; Chen, D. Dual-Modal Photon Upconverting and Downshifting Emissions from Ultra-stable $CsPbBr_3$ Perovskite Nanocrystals Triggered by Co-Growth of Tm:$NaYbF_4$ Nanocrystals in Glass. *ACS Appl. Mater. Interfaces* **2020**, *12*, 18705−18714.

(27) Lin, J.; Yang, C.; Huang, P.; Wang, S.; Liu, M.; Jiang, N.; Chen, D. Photoluminescence Tuning from Glass-Stabilized $CsPbX_3$ (X=Cl, Br, I) Perovskite Nanocrystals Triggered by Upconverting $Tm:KYb_2F_7$ Nanoparticles for High-Level Anti-Counterfeiting. *Chem. Eng. J.* **2020**, *395*, No. 125214.
(28) Zhao, J.; Liu, Y. F.; Zhou, C. P.; Gao, H. P.; Zhang, H. F.; Mao, Y. L. Significantly enhanced luminescence of dual wavelength excitation upconversion nanoparticles by two-dimensional technique. *J. Lumin.* **2020**, *219*, No. 116936.
(29) Li, X.; Cao, F.; Yu, D.; Chen, J.; Sun, Z.; Shen, Y.; Zhu, Y.; Wang, L.; Wei, Y.; Wu, Y.; Zeng, H. All inorganic halide perovskites nanosystem: synthesis, structural features, optical properties and optoelectronic applications. *Small* **2017**, *13*, No. 1603996.
(30) Nedelcu, G.; Protesescu, L.; Yakunin, S.; Bodnarchuk, M. I.; Grotevent, M. J.; Kovalenko, M. V. Fast Anion-Exchange in Highly Luminescent Nanocrystals of Cesium Lead Halide Perovskites ($CsPbX_3$, X = Cl, Br, I). *Nano lett.* **2015**, *15*, 5635−5640.
(31) Yao, W.; Tian, Q.; Wu, W. Tunable emissions of upconversion fluorescence for security applications. *Adv. Opt. Mater.* **2018**, *7*, No. 1801171.
(32) Chen, X.; Yao, W.; Wang, Q.; Wu, W. Designing Multicolor Dual-Mode Lanthanide-Doped $NaLuF_4/Y_2O_3$ Composites for Advanced Anticounterfeiting. *Adv. Opt. Mater.* **2020**, *8*, No. 1901209.
(33) Zhao, J.; Pan, G.; Xu, W.; Jin, S.; Zhang, H.; Gao, H.; Kang, M.; Mao, Y. Strong upconverting and downshifting emission of $Mn^{2+}$ ions in a $Yb,Tm:NaYF_4@NaLuF_4/Mn:CsPbCl_3$ core/shell heterostructure towards dual-model anti-counterfeiting. *Chem. Commun.* **2020**, *56*, 14609−14612.


https://dx.doi.org/10.1021/acs.inorgchem.0c03516
*Inorg. Chem.* 2021, 60, 2649−2655